Current Biology *16*, 625–635, April 4, 2006 DOI 10.1016/j.cub.2006.02.061

Article

Postsynaptic Mad Signaling at the *Drosophila* Neuromuscular Junction

Veronica Dudu,[1] Thomas Bittig,[2] Eugeni Entchev,[1] Anna Kicheva,[1] Frank Jülicher,[2,*] and Marcos González-Gaitán[1,*]

[1] Max Planck Institute of Molecular Cell Biology and Genetics
Pfotenhauer Strasse 108
01307 Dresden
Germany

[2] Max Planck Institute for the Physics of Complex Systems
Nöthnitzer Strasse 38
01187 Dresden
Germany

Summary

Background: Cell-to-cell communication at the synapse involves synaptic transmission as well as signaling mediated by growth factors, which provide developmental and plasticity cues. There is evidence that a retrograde, presynaptic transforming growth factor-β (TGF-β) signaling event regulates synapse development and function in *Drosophila*.

Results: Here we show that a postsynaptic TGF-β signaling event occurs during larval development. The type I receptor Thick veins (Tkv) and the R-Smad transcription factor Mothers-against-dpp (Mad) are localized postsynaptically in the muscle. Furthermore, Mad phosphorylation occurs in regions facing the presynaptic active zones of neurotransmitter release within the postsynaptic subsynaptic reticulum (SSR). In order to monitor in real time the levels of TGF-β signaling in the synapse during synaptic transmission, we have established a FRAP assay to measure Mad nuclear import/export in the muscle. We show that Mad nuclear trafficking depends on stimulation of the muscle.

Conclusions: Our data suggest a mechanism linking synaptic transmission and postsynaptic TGF-β signaling that may coordinate nerve-muscle development and function.

Introduction

During development and in the adult animal, synapses are remodeled in response to genetic programs and environmental cues. This plasticity is thought to be the basis of learning and memory. A model for synaptic plasticity is the *Drosophila* neuromuscular junction (NMJ), which is formed during embryogenesis [1] and grows during larval stages to adjust itself to the growth of the muscle so that it maintains the homeostasis of the synapse [2]. To match the growth of muscle and synapse during larval development, both anterograde communication events (such as synaptic transmission itself) and retrograde signaling take place (reviewed in [3]).

A well-characterized NMJ retrograde signaling event in *Drosophila* is mediated by the TGF-β signaling pathway and is initiated by secretion of the bone morphogenetic protein (BMP)-4-type ligand Glass bottom boat (Gbb) from the muscle [4–9]. Gbb signals upon binding to a presynaptic receptor dimer formed by the type II receptor Wishful thinking (Wit) and one of the type I receptors, either Saxophone (Sax) or Tkv [8]. Gbb binding activates the Ser/Thr kinase activity of the receptor, which phosphorylates the presynaptic transcription factor Mad [4, 5]. The activated signaling molecules are carried from the synapse to the soma by axonal retrograde transport mediated by microtubule motors [7]. In the nuclei, Phospho-Mad (P-Mad) together with the co-Smad Medea (Med) modulates the expression of unknown TGF-β-responsive genes [6]. Through transcriptional control, Gbb retrograde signaling regulates NMJ development and function at three different levels: synaptic transmission between interneurons and motoneurons, growth and differentiation of the NMJ, as well as potentiation of muscle contraction through the secretion of FMRFamide (reviewed in [10–12]).

In the normal *Drosophila* NMJ, synaptic vesicles containing glutamate are docked at specific active zones at the presynaptic membrane, the so-called T-bars. The larval type I synaptic boutons are embedded in the muscle fiber that forms a convoluted specialization of the plasma membrane around the bouton, the subsynaptic reticulum (SSR). Within the SSR, the glutamate receptors (GluRs) cluster opposite to the presynaptic T-bars in a region where both the pre- and postsynaptic membranes are closely attached, the postsynaptic densities (PSDs) [13]. Loss-of-function mutants of the TGF-β signaling pathway (such as *gbb*, *tkv*, *sax*, *wit*, *mad*, and *med*) show a reduced number of synaptic boutons with aberrant morphology, including T-bars floating in the cytoplasm [4–9]. In addition, the pre- and postsynaptic membranes are detached from each other. These morphological phenotypes are accompanied by a reduction of transmitter release [4–9]. Conversely, activation of the pathway has opposite effects: mutations in *daughters-against-dpp* (*dad*), a negative regulator of the TGF-β pathway, as well as the expression of a constitutively active form of Tkv in the neurons induce synaptic overgrowth [8, 9].

The evidence for retrograde TGF-β signaling is based on experiments in which TGF-β signaling mutant phenotypes are rescued by specific expression of a transgene post- or presynaptically: the NMJ phenotype of *gbb* mutants is rescued by expressing a transgenic Gbb in the muscles [7]. However, these experiments suggest that there might also be anterograde/autocrine signaling, since phenotypic rescue improves when Gbb is expressed both by muscles and neurons [7]. Thus, presynaptic Gbb seems to be required to achieve a normal size

*Correspondence: julicher@mpipks-dresden.mpg.de (F.J.); gonzalez@mpi-cbg.de (M.G.-G.)

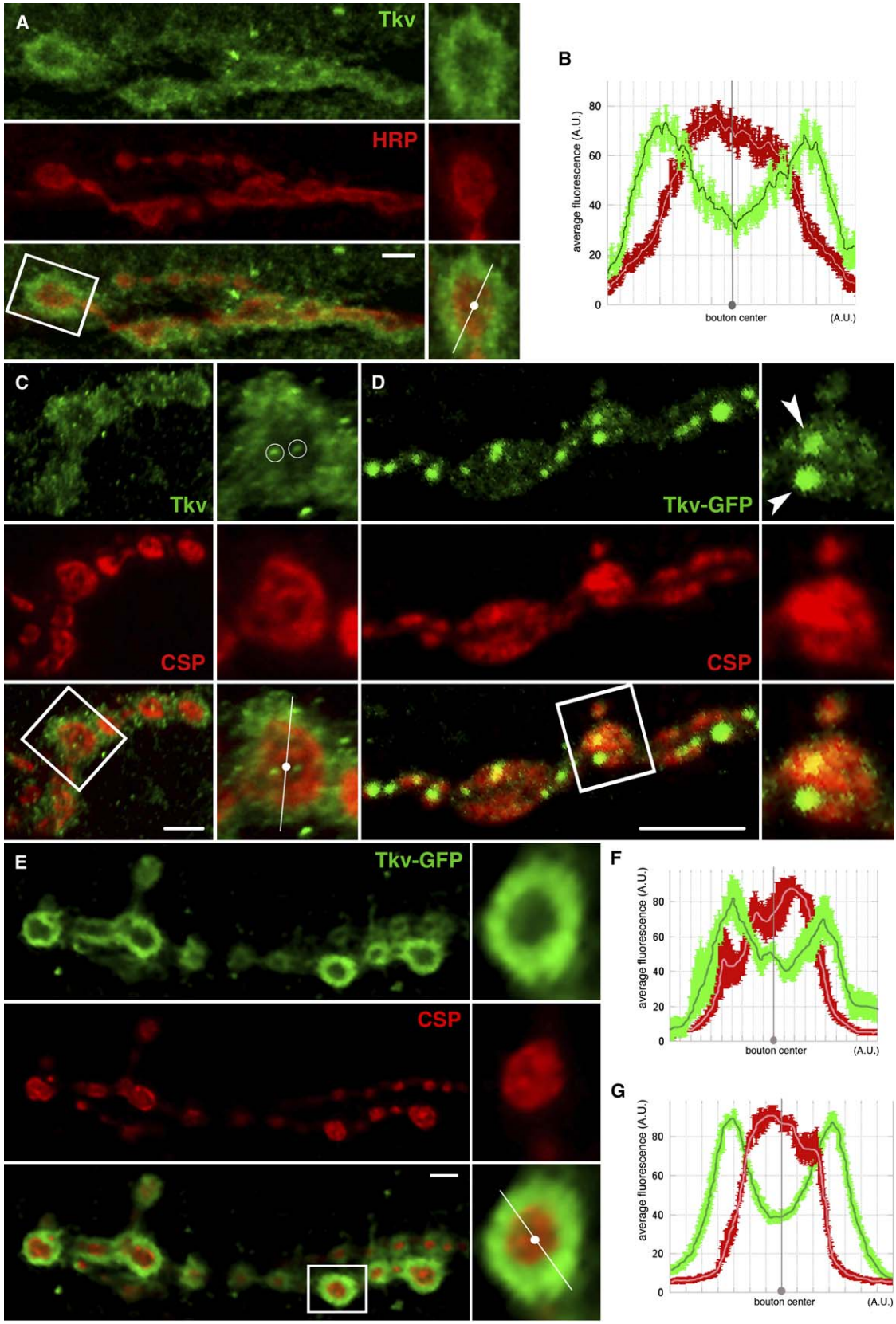

Figure 1. Postsynaptic Tkv

(A, C–E) Double staining of a muscle 6/7 NMJ showing the synaptic boutons labeled by HRP (A) or CSP (C) (red) and endogenous Tkv (green), or CSP (red) and GFP-Tkv (green) expressed either in the neuron (D) or the muscle (E). White boxes indicate the regions enlarged. Note the presynaptic vesicular structures containing Tkv molecules (circle in [C], arrowheads in [D]).

and number of synaptic boutons and a normal quantal content [7]. Therefore, an anterograde/autocrine TGF-β signaling emanating from the neuron could be functionally involved in synaptic growth and performance, in parallel with the well-established retrograde signal.

Here we study this postsynaptic TGF-β signal transduction event at the larval NMJ. We show that, in the muscles, the receptor Tkv is targeted to the postsynaptic plasma membrane where it phosphorylates the transcription factor Mad at the PSD. We also show that Mad nuclear flow in the muscles depends on NMJ depolarization. Our observations imply that an anterograde/autocrine growth factor signaling event mediated by a TGF-β-type ligand might be coupled with synaptic transmission.

Results

Postsynaptic TGF-β Signal Transduction Machinery

In order to study TGF-β signal transduction in the larval NMJs, we first analyzed which integral components of the signaling pathway are present in the muscles and in the central nervous system (CNS) by performing RT-PCR and immunostaining experiments. TGF-β superfamily ligands (Dpp, Gbb, Scw, β-Activin, Alp23B), receptors (Wit, Put, Tkv), and transcription factors (Smox, Mad) are transcribed in the muscle and the brain (see Figure S1 in the Supplemental Data available with this article online) and could in principle mediate TGF-β-like signaling in these organs.

We then determined the subcellular localization of Tkv at the NMJ (Figures 1A–1G). Tkv is found in the synaptic boutons including the SSR surrounding the presynaptic terminal labeled by Horseradish peroxidase (HRP) and cystein-string protein (CSP) (Figures 1A–1C and 1F; for controls of the anti-Tkv antibody specificity, see Figure S2 and [29]). Low levels of Tkv are also detected in vesicular structures within the presynaptic bouton (Figure 1C) and possibly in the presynaptic plasma membrane. Consistently, upon expression of a functional Tkv-GFP chimeric protein in the muscles by the *MHC-Gal4* driver, Tkv is specifically targeted to the SSR (Figures 1E and 1G). Upon panneural Tkv-GFP expression via *elav-Gal4,* the receptor was detected in presynaptic vesicular structures (Figure 1D) and possibly in the presynaptic plasma membrane. The presynaptic localization of the receptor is consistent with the previously reported retrograde TGF-β signaling event at the NMJ [4, 5, 7, 9]. The SSR localization of Tkv raises, on the other hand, the possibility of an additional postsynaptic anterograde/autocrine signaling event.

Postsynaptic Phosphorylation of the R-Smad Mad

Downstream of the Tkv receptors, the signaling cascade is propagated through the activation of the transcription factor R-Smad Mad. Endogenous Mad is found in the synapse as well as in the nuclei of the muscles (Figure 2A; for controls of the anti-Mad antibody specificity, see Figure S3) [30]. In the synapse, endogenous Mad accumulates at the postsynaptic SSR as defined by Discs-large (Dlg) immunostaining (Figures 2A and 2E). At the resolution level of confocal microsocopy, we can not exclude the existence of a pool of Mad at the presynaptic membrane, in accordance with retrograde signaling. Consistently, a functional GFP-Mad chimeric protein, expressed in the muscles, is targeted both to the postsynaptic side of the NMJ in the SSR and to the nuclei (Figures 2B and 2F). Functionality of the GFP-Mad chimera was confirmed by rescuing the lethality of the mad^{B1} null mutant. In summary, both the receptor and the transducing transcription factor of the TGF-β signaling pathway are found in the muscle, consistent with the hypothesis that TGF-β-like signaling takes place postsynaptically.

To address whether signal transduction indeed takes place at the muscle and to determine the site of receptor activation, the localization of phosphorylated Mad (P-Mad) was studied. Figure 2C shows that Mad is found phosphorylated in the muscle nuclei, confirming that signaling takes place at the muscle. Postsynaptically, P-Mad accumulates in a region surrounding the presynaptic terminal. In contrast to the total pool of Mad protein that appears diffuse in the SSR (Figure 2A), the phosphorylated protein concentrates in a punctate postsynaptic pattern that coincides with the PSD, which can be diagnostically labeled by the pattern of glutamate receptor clusters in the muscles (Figures 2C and 2G). The P-Mad/glutamate receptor-positive PSDs appear opposite to the presynaptic active zones, which are diagnostically labeled by nc82 immunostaining (Figures 2D and 2H) [14].

Specificity of the P-Mad staining was confirmed by mad^{12} mutant flies: only small traces of P-Mad staining are detected in the mad^{12} muscle nuclei (Figures 3B and 3C; 5.5% ± 2.0% of the wt level). The Mad^{12} protein is truncated just before the conserved SSVS domain that is phosphorylated by the type I receptor [15]. Low levels of staining at the NMJ (Figures 3B and 3C; 11.0% ± 7.3% of the wt level) are due to residual Mad maternal protein, which allows survival of the mutants until the third instar larval stage [15]. In addition, Mad phosphorylation at the NMJ is reduced upon postsynaptic expression of the i-Smad Dad (26.6% ± 3.8% of the wt level) (Figures 3D and 3E). Nuclear P-Mad is reduced to 28% by postsynaptic expression of Dad and increased by 166% with respect to the control muscles by postsynaptic expression of a constitutively active Tkv receptor (Tkv^{QD}). These data confirm that a transducing event can occur in the muscles. Western blot analysis of P-Mad levels support this observation quantitatively (Figure S4). In addition, postsynaptic expression of Dad causes an increase in the quantal content presynaptically (Figure S6). This effect is probably due to a compensatory presynaptic effect, which might be caused by a defect in the performance of the muscle. No morphological changes of the number of boutons, synaptic area, or muscle size can otherwise be detected at the NMJ (Figure S6). Taken together, these results

(B, F, G) Quantification of endogenous Tkv immunofluorescence (green; [B], n = 15; [F], n = 5) or postsynaptically expressed GFP-Tkv ([G], green; n = 10) and HRP (B) or CSP (F and G) (red) average fluorescence across wt boutons as indicated in the high-magnification insets in (A), (C), and (E). A.U., arbitrary fluorescence units. Bars correspond to standard errors. For details of the quantification, see Experimental Procedures.
Genotypes: (A and C) wt, (D) *elav-GAL4/UAS-Tkv-GFP*, (E) *MHC-GAL4/UAS-Tkv-GFP*. Scale bar equals 5 μm.

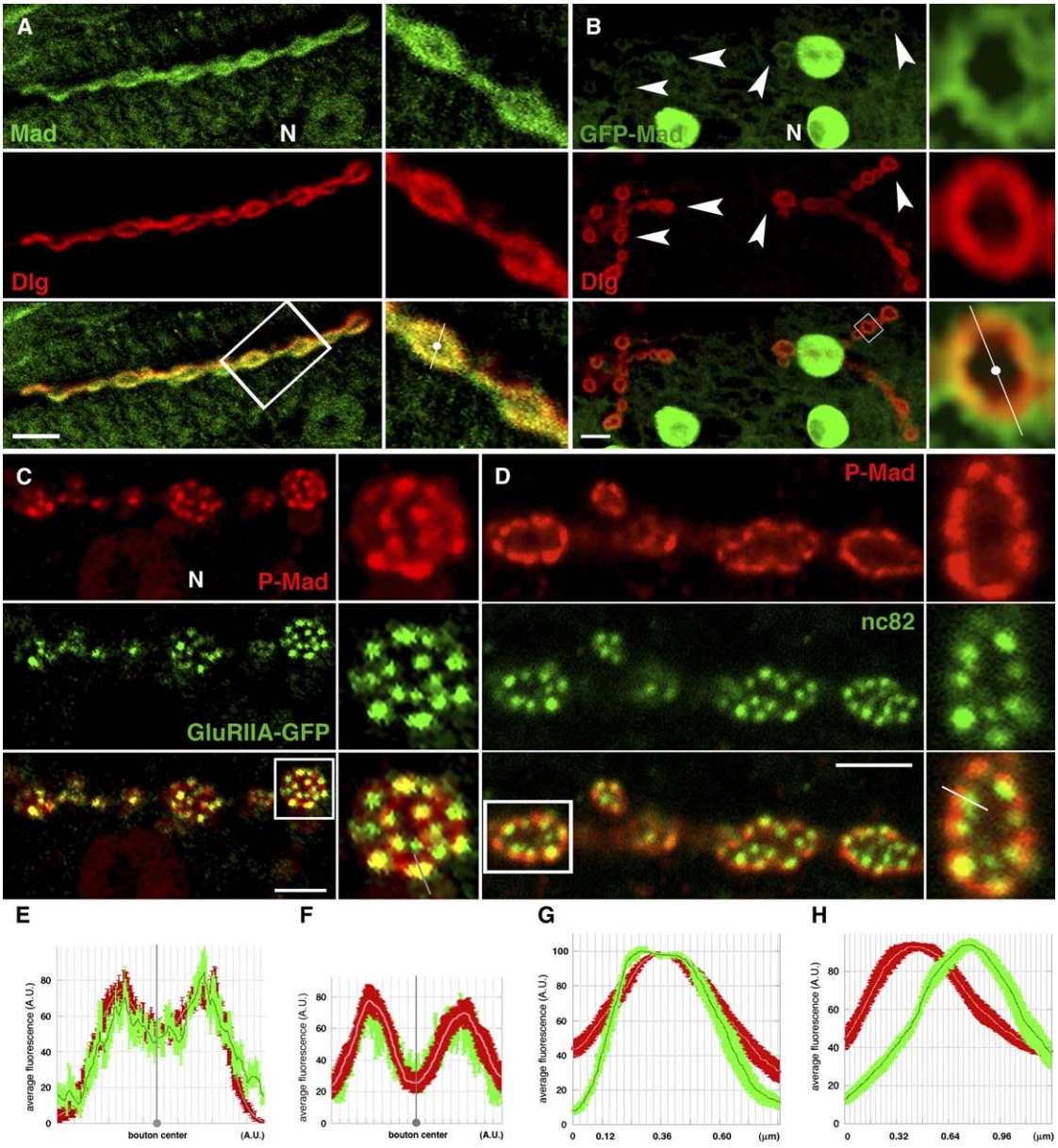

Figure 2. Postsynaptic Mad

(A and B) Double staining of a muscle 6/7 NMJ showing the synaptic boutons labeled in green by endogenous Mad (A) or postsynaptically expressed GFP-Mad (B) and in red by Dlg. White boxes, enlarged regions. N, nucleus.

(C and D) Double staining showing in red phosphorylated Mad immunostaining and in green the glutamate receptor GluRIIA-GFP expressed in the muscle (C) or nc82 labeling the presynaptic active zones (D). White boxes, enlarged regions.

(E and F) Quantification of endogenous Mad immunofluorescence ([E], green; n = 9) or postsynaptically expressed GFP-Mad ([F], green; n = 8) and Dlg (red) average fluorescence across boutons as indicated in the high-magnification insets in (A) and (B). A.U., arbitrary fluorescence units. Bars correspond to standard errors.

(G and H) Quantification of Phospho-Mad fluorescence (red) and postsynaptic GluR ([G], green; n = 12) or presynaptic nc82 ([H], green; n = 12) immunofluorescence across single PSDs as indicated in the high-magnification insets in (C) and (D).

Genotypes: (A and D) wt, (B) *MHC-GAL4/UAS-GFP-Mad*, (C) *MHC-GAL4/UAS-GluRIIA-GFP*. Scale bars equal 5 μm in (C) and (D) and 10 μm in (A) and (B).

indicate that a TGF-β signal at the NMJ causes Mad activation by postsynaptic phosphorylation.

A FRAP Assay to Monitor Synaptic Mad Signaling in Real Time

In order to study the levels of Mad signaling in the postsynaptic terminal in real time during synaptic transmission, we looked at the targeting of GFP-Mad to the boutons in vivo and performed FRAP (fluorescence recovery after photobleaching) experiments to measure its nuclear import/export kinetics. Like the endogenous protein, GFP-Mad can be seen concentrated at the NMJ and in the muscle nuclei (Figure 2B). Upon stimulation with high potassium (K^+) solution, GFP-Mad association

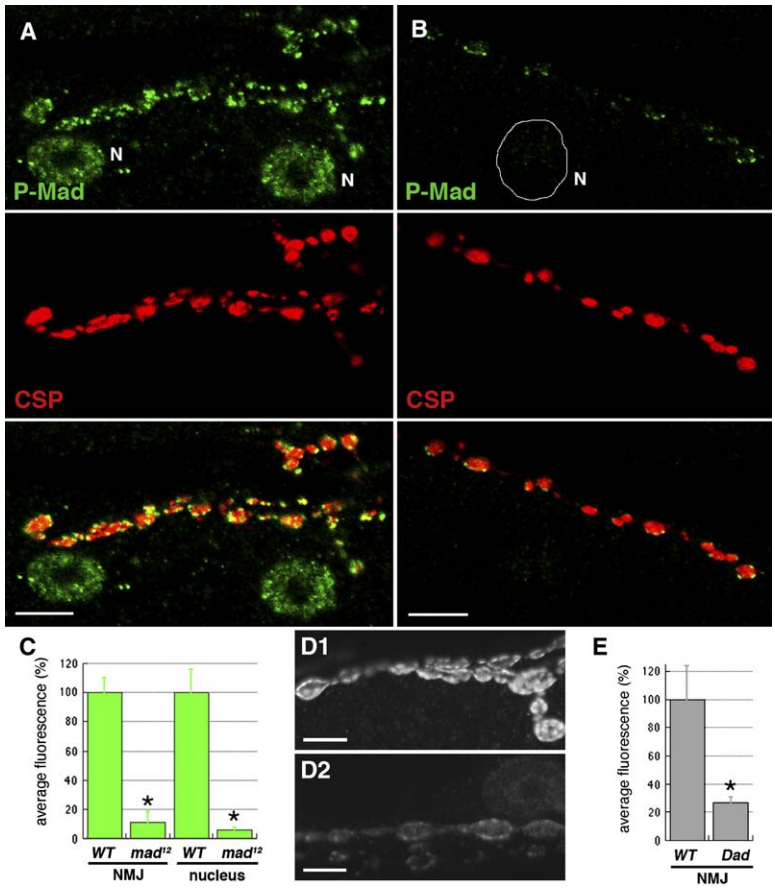

Figure 3. Specificity of the P-Mad Immunostaining

(A and B) Double staining of a muscle 6/7 NMJ showing P-Mad (green) and CSP immunostaining (red) in wt (A) and *mad*^{12} mutants (B). N, nucleus.

(C) Quantification of P-Mad levels of average fluorescence (bars, standard errors) at the NMJ and in the nucleus in wt (n = 7) and *mad*^{12} mutants (n = 8; *p < 0.05).

(D) P-Mad immunostaining in a wt NMJ (D1) and in a NMJ of a muscle expressing Dad (D2).

(E) Quantification of the P-Mad levels of average fluorescence at the NMJ (bars, standard errors) in wt (n = 7) and postsynaptically expressed *Dad* (n = 9; *p < 0.05).

Genotypes: (A and D1) wt, (B) *mad*^{12}/*mad*^{12}, (D2) *MHC-GAL4/UAS-Dad*. Scale bars equal 10 μm (A and B) and 5 μm (D1 and D2).

to the NMJ is increased by 20%–30% (Figure 4A), consistent with the idea that the transcription factor Mad is recruited from the cytosol to the receptors at the SSR during synaptic transmission.

GFP-Mad is mainly concentrated in the nucleus. The nuclei represent only 3.4% of the total volume of the muscle cell, but they accumulate 12% of the total Mad protein (Figure 4B). GFP-Mad can also be seen at lower levels of concentration (3.7 times lower than in the nucleus) in the cytosol (Figure 4C). In muscles expressing the constitutively active Tkv^{QD}, the total amount of protein is unchanged, but the concentration of the protein in the nucleus is elevated by a factor of 3.5 with respect to control muscles (Figures 4B and 4C). Thus, it represents 56% of the total GFP-Mad in the muscle (Figure 4B), implying that more than 50% of cytoplasmic Mad can move into the nucleus upon phosphorylation during constitutive signaling.

Which trafficking step is modified upon phosphorylation to account for Mad nuclear accumulation? Nuclear import, export, or retention in the nucleus of a signaling active phosphorylated Mad pool? In order to distinguish between these possibilities, we established a rapid, real-time assay for Mad postsynaptic signaling based on FRAP. With this assay, we determined the effective nuclear import and export rates, as well as the fraction of Mad molecules that are retained in the nucleus and do not exchange or exchange very slowly with the cytosol: the immobile pool. We reasoned that this immobile fraction may reflect the pool of transcriptionally active phosphorylated Mad (P-Mad*) that is bound to other transcription factors in higher molecular weight complexes and therefore cannot exit the nucleus through the nuclear pore. It is also possible that the active phosphorylated Mad might not be able to exit the nucleus by itself.

The assay consists of bleaching the GFP-Mad fluorescence of the whole nucleus and measuring the kinetics of fluorescence recovery (Figures 4D and 4E). From (1) the kinetics of fluorescence recovery in the nucleus (Figure 4E), (2) the relative steady-state concentrations of GFP-Mad in the nucleus and cytosol before bleaching (Figure 4C), and (3) the size of the immobile fraction (Figure 4H), we determined the effective import and export rates (Figures 4G and 5A; for details, see Experimental Procedures). Knowing the values of these effective rates in the different mutant conditions allowed us to analyze what accounts for the increase in the net accumulation of Mad upon signaling: an increase in nuclear import, a decrease in nuclear export, or both.

In control muscles, the effective import rate of Mad is higher than its export rate (Figure 4G), accounting for the concentration of Mad in the nucleus. Upon constitutive signaling in the Tkv kinase active mutant, the ratio of import to export rates (7.4) is higher than in the control (3.6). This difference in the import/export ratio explains the net accumulation of nuclear Mad in *Tkv*^{QD} muscles above the levels of control in steady state. Interestingly, the effective import rate does not increase, but

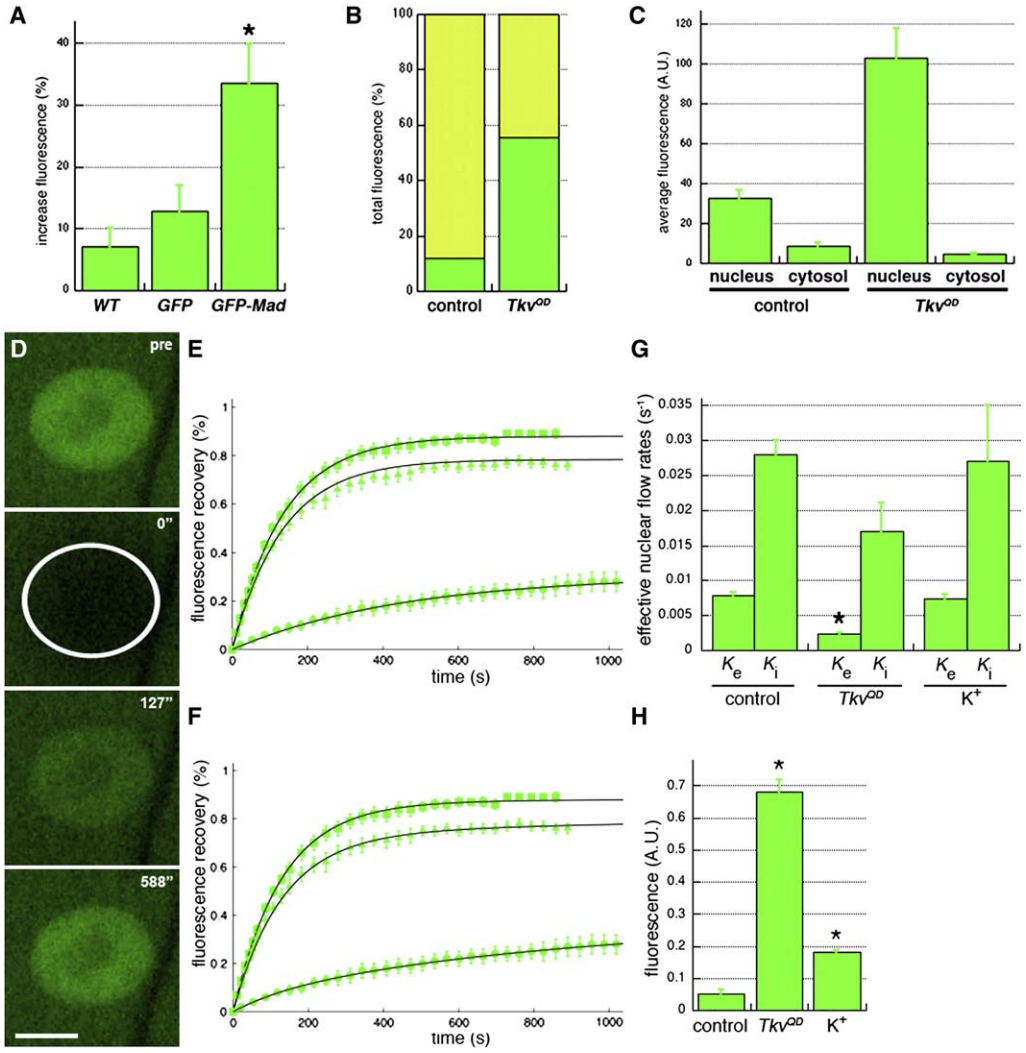

Figure 4. Mad Trafficking at the NMJ

(A) Quantification of the fluorescence increase at the NMJ after high K^+ stimulation in wt (n = 4), *MHC-GAL4/UAS-GFP* control (n = 5), and *MHC-GAL4/UAS-GFP-Mad* (n = 6; *p < 0.05). Bars correspond to standard errors. Note that there is a minor increase in autofluorescence upon stimulation.

(B) Quantification of the total GFP-Mad fluorescence in the muscle nuclei (dark green) and the cytosol (light green) in control and in animals expressing Tkv^{QD} postsynaptically. Genotype: *MHC-GAL4::UAS-GFP-Mad/UAS-Tkv*^{QD}. At least 30 nuclei from more than 4 larvae were measured in each experiment.

(C) Average GFP-Mad concentration in the muscle nuclei and cytosol in control and in animals expressing Tkv^{QD} postsynaptically. Bars correspond to standard errors. At least 30 nuclei from more than 4 larvae were measured in each experiment.

(D) GFP-Mad imaged before (pre) and after fluorescence photobleaching at the indicated times. Genotype: *MHC-GAL4/UAS-GFP-Mad*. Scale bar equals 10 μm.

(E and F) Time course of the fluorescence recovery. Fluorescence recovery is normalized to the prebleach value and the bleaching depth (see Experimental Procedures). Fitting curves correspond to the single-exponential ([E]; equation 4; see Experimental Procedures) or double exponential ([F]; equation 2) fit. For further details, see Supplemental Data (equations 8 and 14). The value of the standard error is represented for data at least every 30 s, to indicate the robustness of the data set. Square, control; triangle, K^+; circle, Tkv^{QD}.

(G) Effective nuclear export (K_e) and import (K_i) rates in control, Tkv^{QD}, and upon K^+ stimulation. *p < 0.05. Bars correspond to standard errors.

(H) Size of the immobile GFP-Mad pool in control, Tkv^{QD}, and upon K^+ stimulation. *p < 0.05. Bars correspond to standard errors. Sample size (E–H): control, n = 5; Tkv^{QD}, n = 6; K^+, n = 7.

decreases slightly upon constitutive signaling (1.6 times smaller in Tkv^{QD} than in control), while it is the effective export rate that significantly decreases (3.4 times smaller in Tkv^{QD}). These data imply that the increase in the net nuclear accumulation of Mad during signaling is explained by a decrease in the export rate, rather than by an increase in the import rate.

We also analyzed the size of the Mad immobile pool in the FRAP experiments (Figure 4H). In control muscles, only 5% of nuclear GFP-Mad is immobile, suggesting low levels of Mad signaling in the resting synaptic terminal. In contrast, constitutive signaling caused by expression of Tkv^{QD} leads to an increase by an order of magnitude (67%) of the immobile pool of Mad in the nucleus.

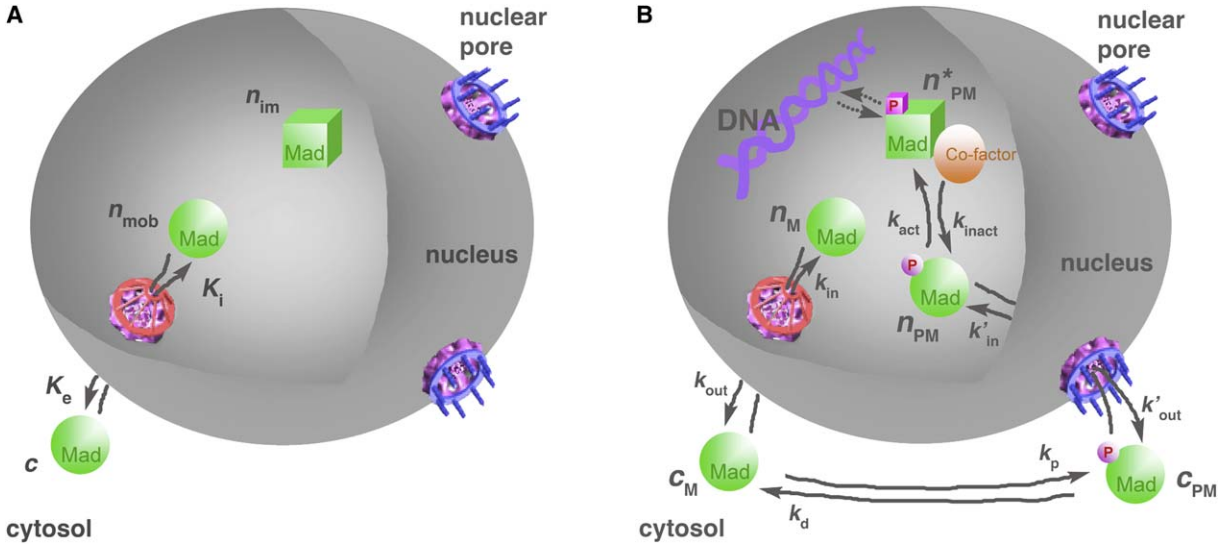

Figure 5. Models of Mad Nuclear/Cytoplasmic Trafficking in the Muscle

(A) A simplified model for Mad trafficking. Cytosolic Mad (*c*) enters the nucleus through the nuclear pore with a rate K_i. Inside the nucleus there are two Mad populations: an immobile one, n_{im}, and a mobile one, n_{mob}, which exits the nucleus with a rate K_e.

(B) A model considering different specific import/export rates for Mad and P-Mad. Mad and P-Mad enter/exit the nucleus through the nuclear pore with different rates; inside the nucleus, P-Mad becomes activated and binds to cofactors, and this high molecular complex can not cross the nuclear pore, accounting thus for the immobile pool. For a definition of the various Mad pools and rates, see text and Supplemental Data.

This result is consistent with higher levels of P-Mad* in the Tkv^{QD} condition.

Thus, the FRAP assay can be used to assess in real time (within minutes) the state of Mad activation by determining the changes caused by the signaling event on the effective rates of Mad nuclear import and export as well as the size of the nuclear immobile pool. We therefore used the FRAP assay to determine the changes in the level of Mad activation during synaptic transmission.

In order to study the effects of postsynaptic stimulation on the nuclear import/export kinetics, we incubated the larvae with high potassium (K^+) solution for 90 s, washed out the K^+ solution, and subsequently bleached the fluorescence of a whole nucleus. We then monitored the fluorescence recovery. In this situation, the kinetic parameters shift slowly from those characterizing the steady state of a resting muscle to those corresponding to a stimulated muscle. Upon high K^+ stimulation, the effective import and export rates do not suffer a major change compared to the values in resting muscles (Figure 4G). In contrast, the pool of immobilized GFP-Mad molecules increases by a factor of 4 (up to 19% of the nuclear Mad) with respect to the size of the immobile pool before stimulation (Figure 4H). This increase suggests that the level of Mad signaling is increased during synaptic transmission and depolarization of the muscle. Also, it implies that growth factor postsynaptic signaling might be coupled to synaptic activity, consistent with an instructive role of the neural activity for the development of the muscle.

A Kinetic Model for Mad Signaling in the Muscle

Nuclear accumulation of R-Smad transcription factors in response to TGF-β is triggered by receptor-mediated phosphorylation [16]. This in turn implies that phosphorylated R-Smads show different nuclear import/export rates than the nonphosphorylated molecules. In addition, the state of activation of the receptor kinase modifies the relative amounts of phosphorylated versus nonphosphorylated R-Smad. In the analysis described above, the observed GFP fluorescence corresponds to the sum of the fluorescence signal of the two species of Mad (Mad and P-Mad). Therefore, the level of Mad nuclear flow in a particular experiment results from the relative contribution of the specific import and export rates of phosphorylated and nonphosphorylated Mad as well as the relative pool size of these two species.

We propose a model that captures the effect of phosphorylation rate changes on the flow of Mad molecules into the nucleus (Figure 5B). In this model we assume: (1) that the specific import and export rates of Mad and P-Mad are constant, (2) that the only rate that changes in the different experiments is the phosphorylation rate (k_p), and (3) that there is a nuclear pool of P-Mad* molecules (of concentration n^*_{PM}) associated with slow exchange rates (k_{act} and k_{inact}). This P-Mad* pool accounts for the existence of an immobile nuclear GFP-Mad fraction. Since the volume of the cytosol is 600 times larger than that of a single bleached nucleus, we also assumed that, after bleaching, the concentrations of the cytosolic Mad species remain constant. As a consequence of the slow exchange rates related to P-Mad*, we consider n^*_{PM} to be constant in the time scale of the experiment (1000 s). We also neglect the de novo production and degradation of Mad as well as nuclear dephosphorylation within the 1000 s of the experiment. It is worth noting here that signaling might in reality affect some of the rates considered constant in this model in addition to the effect on the phosphorylation rate. We neglect these possible effects for the sake of simplicity of the model.

Under these assumptions, the FRAP kinetics can be described by the following equations:

$$\frac{dn_M}{dt} = k_{in}c_M - k_{out}n_M$$
$$\frac{dn_{PM}}{dt} = k'_{in}c_{PM} - k'_{out}n_{PM} \quad (1)$$
$$\frac{dn^*_{PM}}{dt} = 0,$$

where n_M is the concentration of nuclear Mad, n_{PM} is the concentration of nuclear P-Mad, c_M is the concentration of cytosolic Mad, c_{PM} is the concentration of cytosolic P-Mad, k_{in} is the import rate of cytosolic Mad into the nucleus, k_{out} is the export rate of Mad from the nucleus, k'_{in} is the import rate of cytosolic P-Mad into the nucleus, and k'_{out} is the export rate of P-Mad from the nucleus.

The normalized fluorescence recovery curves (Figure 4F; for normalization see Experimental Procedures) are fit to the expression:

$$F(t) = \frac{n^s_M}{n^s_{tot}}(1-b)(1-e^{-k_{out}t}) + \frac{n^s_{PM}}{n^s_{tot}}(1-b)(1-e^{-k'_{out}t}), \quad (2)$$

which is derived from equations 1. Here, F is the total nuclear fluorescence normalized to the bleaching depth (b, the fraction of nonbleached molecules) and the prebleach value, and the quantities n^s_M, n^s_{PM}, and n^s_{tot} account for the steady-state concentration of nuclear Mad, nuclear P-Mad, and total nuclear Mad, respectively (see also Supplemental Data). Note that the double exponential equation 2 depends only on the concentrations of Mad and P-Mad in the nucleus and their respective export rates.

We fit the data from the three different FRAP experimental conditions (control, Tkv^{QD}, and K^+) to the double exponential equation 2 assuming that in the different experiments the phosphorylation rate (k_p) is the only changing rate. We find that in the case of Tkv^{QD}, the phosphorylation rate has to increase 230-fold with respect to control, assuming that all the other rates are fixed (Table 1). This leads to a 17 times higher level of steady-state mobile P-Mad in the nucleus (Table 1). The K^+ stimulation increases the phosphorylation rate by a factor of 5 with respect to resting NMJ, and the nuclear P-Mad concentration 4 times. These data, together with the analysis of the immobile fraction, support the idea that Mad signaling is increased upon stimulation of the muscle.

This analysis also allows the determination of the specific import and export rates for the two species Mad and P-Mad, as well as their relative fractions in the nucleus and the cytosol (Table 1; see Supplemental Data for data analysis leading to these values). Interestingly, the specific import rate of P-Mad is about 2 times smaller than for Mad, while the specific export rate for P-Mad is much smaller (7-fold; Table 1) compared to the nonphosphorylated protein. Consistent with the analysis of the effective rates (Figure 4), these results (Table 1) imply that the observed net flow into the nucleus upon phosphorylation is caused by a decrease in the export rate of Mad, rather than by an increase in its import into the nucleus.

Table 1. Mad Pools and Specific Rates Describing Mad Trafficking

	Control	Tkv^{QD}	K^+	Units
k_{in}		**0.028**		s^{-1}
k_{out}		**0.0078**		s^{-1}
k'_{in}		**0.016**		s^{-1}
k'_{out}		**0.0011**		s^{-1}
k_{act}/k_{inact}		**1.68**		—
k_p/k_d	0.0052	1.21	0.028	—
n^s_M/n^s_{tot}	0.945	0.070	0.764	—
n^s_{PM}/n^s_{tot}	0.020	0.347	0.088	—
$(n^s_M + n^s_{PM})/n^s_{tot}$	0.965	0.417	0.852	—
c^s_M/c^s_{tot}	0.995	0.453	0.972	—
c^s_{PM}/c^s_{tot}	0.005	0.547	0.028	—

Specific rates and pool sizes of Mad and PMad in unstimulated controls, Tkv^{QD}-expressing mutants, and K^+ stimulated muscles. Note that for control, Tkv^{QD}, and K^+ muscles, the specific rates of Mad and P-Mad import and export as well as the exchange rates of the mobile/immobile nuclear fraction (bold) are the same.

Discussion

Molecular signals are often transmitted in the reverse direction across the synapse to regulate the structure and function of the presynaptic neuron [17]. There is now good evidence that BMP-type TGF-β ligands are essential retrograde signaling ligands in the *Drosophila* nervous system [4–6, 8, 18, 19] and that they control synaptic growth, synaptic function, and in some cases the specificity of the particular neurotransmitter released at the synaptic terminal [4–8, 18–24]. Our data show that there is an additional postsynaptic TGF-β signaling cascade at the NMJ that is consistent with anterograde and/or autocrine signaling. Four lines of evidence support the existence of a postsynaptic signaling event: (1) core transduction components of the BMP-type signaling pathway, such as the receptor Tkv and the transcription factor Mad, are present in the muscle where they accumulate in the SSR (Figures 1 and 2), (2) phosphorylation of Mad takes place in the PSD, opposite to the presynaptic active zones where exocytosis of neurotransmitter takes place (Figure 2), (3) a FRAP-based assay that monitors signaling-dependent nuclear import/export and nuclear retention of Mad revealed that Mad-mediated signaling can take place in the muscle (Figure 4), and (4) upon stimulation of the muscle, Mad targeting to the terminal is enhanced and the levels of postsynaptic Mad signaling are increased, as monitored with the FRAP assay (Figure 4).

Taken together, these data are consistent with the existence of an anterograde signaling event that is initiated in the presynaptic terminal through exocytosis of a TGF-β-type ligand. Binding of the ligand to the Tkv receptor at the PSD would then lead to activation of the receptor and thereby phosphorylation of Mad. Phosphorylation of Mad causes a decrease in the nuclear export of the transcription factor and thereby its accumulation in the muscle nuclei. Nuclear P-Mad in turn mediates transcriptional control of the target genes of the signaling pathway. Thus, while retrograde BMP signaling instructs the neurons about the physiological and developmental state of the muscle, such an anterograde signaling event may provide the muscle with information about the activity of the neuron in the medium/long term.

However, these observations do not rule out an autocrine BMP signaling event: a ligand (perhaps, again, Gbb) released from the muscle at the synaptic site could activate signaling in the muscle itself. Clearly, further analysis needs to be carried out to discriminate between these two possibilities.

Mad Nuclear Immobile Fraction and Signaling

We have established a FRAP assay to determine in real time the state of activation of TGF-β pathway in the muscle. This assay is useful to study rapid events such as synaptic transmission, where it is desirable to capture fast changes in the state of signaling. The FRAP experiments allow us to determine the rates of nuclear import/export of Mad and the size of the nuclear Mad pool that does not exchange (or exchanges slowly) with the cytosol: the immobile fraction. Experiments in which the levels of signaling are affected reveal that both the effective import/export rates and the size of the immobile fraction correlate with the signaling state: higher levels of signaling can be associated with a larger Mad immobile pool in the nucleus and higher import-to-export ratio.

What is the molecular meaning of the correlation between signaling and the immobile pool? We first considered that the nuclear P-Mad binds/unbinds to the DNA with rates that are slower than other rates during signaling (phosphorylation/dephosphorylation, import/export) and does not significantly contribute to the recovery in the 1000 s time of the experiments. Bound to the DNA, P-Mad could not exchange with the cytosol, and the relatively slow rates of binding/unbinding would generate an immobile fraction as shown in the FRAP experiment. Further experiments, however, did not support this hypothesis. After bleaching GFP-Mad in a small region within the nucleus in a Tkv^{QD}-expressing muscle (where 67% of the nuclear Mad does not exchange with the cytosol), the fluorescence fully recovered within this bleached region (Figures S5B and S5D), revealing that Mad is not immobilized within the nucleus. Is then the DNA moving within the nucleus? FRAP experiments with Histone2A-GFP discard the possibility that the DNA in the nucleus is moving rapidly and show that it remains immobile during the time scale of the FRAP experiments (Figures S5C and S5D).

What could then explain the correlation between signaling and immobile pool? We speculate that P-Mad associates with other cofactors in the nucleus with slow binding and unbinding rates. Engaged in a macromolecular complex, P-Mad would be unable to exit the nucleus through the nuclear pore and thereby would generate the immobile pool revealed in the FRAP experiments.

Mad Postsynaptic Signaling: Development and Physiology of the Synapse

Retrograde signaling has been proposed to convey information to the neuron about the development of the muscle, so that the presynaptic terminal and the muscle grow synchronously and the increase of the SSR is coordinated with the appearance of new boutons and active zones [2]. What could then be the role of anterograde Mad signaling in the muscle? We speculate that upon synaptic transmission, a quantum of neurotransmitter is released together with a "quantum" of growth factor from the presynaptic vesicles. If this is true, postsynaptic signaling coupled to synaptic activity could endow the muscle with information about the activity of the neuron and thereby control the growth and development of the NMJ. It will be interesting, therefore, to study at the ultrastructural level whether the same vesicles that contain the neurotransmitter contain the TGF-β growth factor.

Conclusions

Our data show that postsynaptic TGF-β signaling occurs at the NMJ. Furthermore, our data suggest a coupling between muscle stimulation and postsynaptic TGF-β signaling. Such coupled processes may confer information to the muscle about the activity of the neuron during development.

Experimental Procedures

Drosophila Stocks

The following *Drosophila* stocks have been used: wild-type OreR, mad^{12} [25], *UAS-Dad* [26], *UAS-GluRIIA-GFP* [13], $UAS\text{-}Tkv^{QD}$ [27], *UAS-GFP* (Barry Dickson, Institute of Molecular Pathology, Vienna, Austria), and *UAS-His2Av-GFP* [28]. *UAS-Tkv-GFP* flies were generated by subcloning the coding sequence of Tkv (LD15534; fly genome project) into pUAST containing EGFP downstream of the insertion. For the *UAS-GFP-Mad* flies, the coding sequence of Mad (RE72705) was subcloned into pUAST containing EGFP upstream of the insertion.

Antibodies and Immunocytochemistry

Antibodies used: rabbit anti-Tkv, 1:500 [29]; rabbit anti-Mad, 1:100 [30]; mouse anti-Dlg, 1:500 (4F3, Hybridoma Bank); rabbit anti-P-Mad, 1:1000 [31]; mouse anti-CSP, 1:100 [32]; mouse anti-nc82, 1:100 [33]; goat anti-HRP, 1:100 (Sigma); rabbit anti-GFP, 1:200 (Santa Cruz). Corresponding secondary Alexa 488, 546, and 633-conjugated antibodies (Molecular Probes) were used 1:500 diluted. Preparation and immunostainings of third instar larvae NMJs were performed as previously described [14, 34]. Images were acquired with a Zeiss LSM510 confocal microscope and processed with Adobe Photoshop 7.0 (Adobe Systems). Analysis was restricted to synapses of muscles 6/7 in abdominal segments 2 to 4 (A2-A4).

Fluorescence Recovery after Photobleaching Experiments

For in vivo imaging, third instar larvae were dissected in ice-cold Ca^{2+}-free saline [35] to prevent movement. FRAP experiments were performed with *MHC-GAL4/UAS-GFP-Mad* (referred to as control in all FRAP experiments) and *MHC-GAL4::UAS-GFP-Mad/UAS-*Tkv^{QD} (referred to as Tkv^{QD}) larvae on a LSM510 laser scanning confocal microscope. GFP was excited with the 488 nm Argon laser line and emission was monitored between 505 and 530 nm. During recording, third instar larvae were maintained in HL3 saline [36].

In the GFP-Mad muscles, the fluorescence of a nucleus (Figure 4) or a small region (Figure S5) within the nucleus was bleached by the 488 nm laser line at full laser power. The muscles were imaged with low levels of 488 nm excitation light to avoid bleaching of GFP signal. Recordings were performed for 200 to 1000 s, with time-lapse interval of 11 s. For synaptic stimulation experiments, high K^+ saline (90 mM KCl, 80 mM NaCl, 5 mM HEPES, 2 mM $MgCl_2$, 2 mM $CaCl_2$, 36 mM sucrose [pH 7.3]) was applied for 1.5 min to third instar *MHC-GAL4/UAS-GFP-Mad* larvae (referred to as K^+ in all FRAP experiments), then replaced with HL3 saline and the FRAP was performed as described above. The average fluorescence intensity in the bleached area was monitored with the Zeiss software. The fluorescence intensity $I(t)$ was normalized according to:

$$F(t) = \frac{I(t) - I(0)}{I_0}, \quad (3)$$

where $I(0)$ is the fluorescence intensity immediately after bleaching and I_0 is the fluorescence intensity before bleaching.

The recovery of the fluorescence *F(t)* was fitted to the following equation:

$$F(t) = m(1 - b)(1 - e^{-K_e t}), \quad (4)$$

where m is the mobile fraction, $b = I(0)/I_0$ is the experimental fraction of unbleached molecules, K_e is the effective export rate, and t is time after bleaching (see Supplemental Data for derivation of this formula). The nuclear effective export rates K_e and the mobile fractions m were determined directly by fitting the recovery curves from each individual experiment to the above equation by Mathematica software (Wolfram Research). The values K_e and m were determined in each experiment and averaged. At least five experiments were performed for each mutant condition.

Since 1000 s after bleaching the mobile nuclear and cytosolic pools are close to equilibrium, the effective nuclear import rate of Mad can be defined as:

$$K_i = mK_e n^s_{tot}/c^s, \quad (5)$$

where n^s_{tot} and c^s are the average steady-state concentrations of nuclear and cytoplasmic Mad, respectively, determined in an independent experimental set.

Quantifications

The postsynaptic localization of Tkv, Tkv-GFP, Mad, and GFP-Mad (Figures 1B, 1F, 1G, 2E, and 2F) was monitored by quantifying their immunofluorescence signal with LSM5 Image Examiner, across 5–15 boutons belonging to at least three different preparations (along a segment that encompasses the pre- and postsynaptic areas and extends an additional 0.5 μm outside the postsynaptic area). The length of this segment was normalized to the maximum length, and the fluorescence signal was normalized to 100% for the maximum value in each sample. HRP, CSP, and Dlg immunofluorescence were used as pre- and postsynaptic markers, respectively. Similarly, the postsynaptic localization of Phospho-Mad (Figures 2G and 2H) was monitored by quantifying its immunofluorescence signal with respect to the GluR and nc82 fluorescence signal. The signal of P-Mad fluorescence (Figures 3C and 3E) was analyzed in at least seven synapses belonging to at least three preparations of wt, *mad*^{12}/*mad*^{12}, and *MHC-GAL4/UAS-Dad*. The total intensity of the signal in the synaptic area was measured in ImageJ (NIH). GFP fluorescence at the synapse (Figure 4A) was imaged live on a Zeiss upright LSM510 microscope. At least four preparations of wt, *MHC-GAL4/UAS-GFP*, and *MHC-GAL4/UAS-GFP-Mad* were imaged before and after stimulation with high K^+ solution (60 mM KCl) for 5 min. The synapses were double labeled with FM4-64 (Molecular Probes), which accumulates in the convoluted membranes of the SSR. The increase in average fluorescence at the NMJ upon synaptic stimulation was analyzed with ImageJ. GFP-Mad fluorescence in the cytosol and nuclei of the muscles (Figure 4) was analyzed in at least six preparations of *MHC-GAL4/UAS-GFP-Mad* (control), *MHC-GAL4/UAS-GFP-Mad* after incubation with high K^+ solution (K^+), and *MHC-GAL4::UAS-GFP-Mad/UAS-Tkv*^{QD} (*Tkv*^{QD}). The average intensity of the signal was measured with LSM5 Image Examiner.

Imaging conditions were such that the detected fluorescence is linearly related to the concentration. This was checked in a series of experiments in which the GFP preparation was repeatedly bleached. In each bleaching step, fluorescence decreased by the same percentage, confirming that fluorescence and concentration are linearly related. For all the graphs the standard errors are plotted. The statistical significance of the data was analyzed with InStat (GraphPad).

Electrophysiology

Electrophysiology was performed according to a standard protocol [14, 34]. For further details, see Figure S6.

Supplemental Data

Supplemental Data include six figures and Supplemental Experimental Procedures and can be found with this article online at http://www.current-biology.com/cgi/content/full/16/7/625/DC1/.

Acknowledgments

We thank C.P. Heisenberg and N. Foster for critical reading and comments on the manuscript. We are indebted to Tanja and Christian Rosenmund as well as to Luis Pardo for their help in the electrophysiology. Our thanks also to P. Pantazis for the helpful discussions and to D. Backasch and A. Schwabedissen for the excellent technical assistance. This work was supported by the Max Planck Society, HFSP, and Deutsche Forschungsgemeinschaft.

Received: November 14, 2005
Revised: February 15, 2006
Accepted: February 17, 2006
Published: April 3, 2006

References

1. Broadie, K., and Bate, M. (1993). Activity-dependent development of the neuromuscular synapse during *Drosophila* embryogenesis. Neuron *11*, 607–619.
2. Schuster, C.M., Davis, G.W., Fetter, R.D., and Goodman, C.S. (1996). Genetic dissection of structural and functional components of synaptic plasticity. II. Fasciclin II controls presynaptic structural plasticity. Neuron *17*, 655–667.
3. Koh, Y.H., Gramates, L.S., and Budnik, V. (2000). *Drosophila* larval neuromuscular junction: molecular components and mechanisms underlying synaptic plasticity. Microsc. Res. Tech. *49*, 14–25.
4. Aberle, H., Haghighi, A.P., Fetter, R.D., McCabe, B.D., Magalhães, T.R., and Goodman, C.S. (2002). *wishful thinking* encodes a BMP type II receptor that regulates synaptic growth in *Drosophila.* Neuron *33*, 545–558.
5. Marqués, G., Bao, H., Haerry, T.E., Shimell, M.J., Duchek, P., Zhang, B., and O'Connor, M.B. (2002). The *Drosophila* BMP type II receptor Wishful Thinking regulates neuromuscular synapse morphology and function. Neuron *33*, 529–543.
6. McCabe, B.D., Hom, S., Aberle, H., Fetter, R.D., Marques, G., Haerry, T.E., Wan, H., O'Connor, M.B., Goodman, C.S., and Haghighi, A.P. (2004). Highwire regulates presynaptic BMP signaling essential for synaptic growth. Neuron *41*, 891–905.
7. McCabe, B.D., Marques, G., Haghighi, A.P., Fetter, R.D., Crotty, M.L., Haerry, T.E., Goodman, C.S., and O'Connor, M.B. (2003). The BMP homolog Gbb provides a retrograde signal that regulates synaptic growth at the *Drosophila* neuromuscular junction. Neuron *39*, 241–254.
8. Rawson, J.M., Lee, M., Kennedy, E.L., and Selleck, S.B. (2003). *Drosophila* neuromuscular synapse assembly and function require the TGF-β type I receptor saxophone and the transcription factor Mad. J. Neurobiol. *55*, 134–150.
9. Sweeney, S.T., and Davis, G.W. (2002). Unrestricted synaptic growth in *spinster*—a late endosomal protein implicated in TGF-β-mediated synaptic growth regulation. Neuron *36*, 403–416.
10. Keshishian, H., and Kim, Y.S. (2004). Orchestrating development and function: retrograde BMP signaling in the *Drosophila* nervous system. Trends Neurosci. *27*, 143–147.
11. Marqués, G. (2005). Morphogens and synaptogenesis in *Drosophila.* J. Neurobiol. *64*, 417–434.
12. Salinas, P.C. (2005). Signaling at the vertebrate synapse: new roles for embryonic morphogens? J. Neurobiol. *64*, 435–445.
13. Rasse, T.M., Fouquet, W., Schmid, A., Kittel, R.J., Mertel, S., Sigrist, C.B., Schmidt, M., Guzman, A., Merino, C., Qin, G., et al. (2005). Glutamate receptor dynamics organizing synapse formation in vivo. Nat. Neurosci. *8*, 898–905.
14. Wucherpfennig, T., Wilsch-Bräuninger, M., and González-Gaitán, M. (2003). Role of *Drosophila* Rab5 during endosomal trafficking at the synapse and evoked neurotransmitter release. J. Cell Biol. *161*, 609–624.
15. Raftery, L.A., Twombly, V., Wharton, K., and Gelbart, W.M. (1995). Genetic screens to identify elements of the decapentaplegic signaling pathway in *Drosophila.* Genetics *139*, 241–254.
16. Xu, L., Chen, Y.G., and Massagué, J. (2000). The nuclear import function of Smad2 is masked by SARA and unmasked by TGF-β-dependent phosphorylation. Nat. Cell Biol. *2*, 559–562.

17. Fitzsimonds, R.M., and Poo, M.M. (1998). Retrograde signaling in the development and modification of synapses. Physiol. Rev. *78*, 143–170.
18. Haghighi, A.P., McCabe, B.D., Fetter, R.D., Palmer, J.E., Hom, S., and Goodman, C.S. (2003). Retrograde control of synaptic transmission by postsynaptic CaMKII at the *Drosophila* neuromuscular junction. Neuron *39*, 255–267.
19. Marqués, G., Haerry, T.E., Crotty, M.L., Xue, M., Zhang, B., and O'Connor, M.B. (2003). Retrograde Gbb signaling through the Bmp type 2 receptor wishful thinking regulates systemic FMRFa expression in *Drosophila.* Development *130*, 5457–5470.
20. Allan, D.W., St Pierre, S.E., Miguel-Aliaga, I., and Thor, S. (2003). Specification of neuropeptide cell identity by the integration of retrograde BMP signaling and a combinatorial transcription factor code. Cell *113*, 73–86.
21. Arora, K., O'Connor, M.B., and Warrior, R. (1996). BMP signaling in *Drosophila* embryogenesis. Ann. N Y Acad. Sci. *785*, 80–97.
22. Cho, K.W., and Blitz, I.L. (1998). BMPs, Smads and metalloproteases: extracellular and intracellular modes of negative regulation. Curr. Opin. Genet. Dev. *8*, 443–449.
23. Christian, J.L. (2000). BMP, Wnt and Hedgehog signals: how far can they go? Curr. Opin. Cell Biol. *12*, 244–249.
24. Liu, F. (2003). Receptor-regulated Smads in TGF-β signaling. Front. Biosci. *8*, s1280–s1303.
25. Sekelsky, J.J., Newfeld, S.J., Raftery, L.A., Chartoff, E.H., and Gelbart, W.G. (1995). Genetic characterization and cloning of *Mothers against dpp*, a gene required for *decapentaplegic* function in *Drosophila melanogaster.* Genetics *139*, 1347–1358.
26. Tsuneizumi, K., Nakayama, T., Kamoshida, Y., Kornberg, T.B., Christian, J.L., and Tabata, T. (1997). Daughters against dpp modulates *dpp* organizing activity in *Drosophila* wing development. Nature *389*, 627–631.
27. Haerry, T.E., Khalsa, O., O'Connor, M.B., and Wharton, K.A. (1998). Synergistic signaling by two BMP ligands through the SAX and TKV receptors controls wing growth and patterning in *Drosophila.* Development *125*, 3977–3987.
28. Clarkson, M., and Saint, R. (1999). A His2AvDGFP fusion gene complements a lethal His2AvD mutant allele and provides an in vivo marker for *Drosophila* chromosome behavior. DNA Cell Biol. *18*, 457–462.
29. Kruse, K., Pantazis, P., Bollenbach, T., Jülicher, F., and González-Gaitán, M. (2004). Dpp gradient formation by dynamin-dependent endocytosis: receptor trafficking and the diffusion model. Development *131*, 4843–4856.
30. Sutherland, D.J., Li, M., Liu, X.Q., Stefancsik, R., and Raftery, L.A. (2003). Stepwise formation of a SMAD activity gradient during dorsal-ventral patterning of the *Drosophila* embryo. Development *130*, 5705–5716.
31. Tanimoto, H., Itoh, S., ten Dijke, P., and Tabata, T. (2000). Hedgehog creates a gradient of DPP activity in *Drosophila* wing imaginal discs. Mol. Cell *5*, 59–71.
32. Zinsmaier, K.E., Eberle, K.K., Buchner, E., Walter, N., and Benzer, S. (1994). Paralysis and early death in cysteine string protein mutants of *Drosophila.* Science *263*, 977–980.
33. Heimbeck, G., Bugnon, V., Gendre, N., Haberlin, C., and Stocker, R.F. (1999). Smell and taste perception in *Drosophila melanogaster* larva: toxin expression studies in chemosensory neurons. J. Neurosci. *19*, 6599–6609.
34. Guichet, A., Wucherpfennig, T., Dudu, V., Etter, S., Wilsch-Brauniger, M., Hellwig, A., González-Gaitán, M., Huttner, W.B., and Schmidt, A.A. (2002). Essential role of endophilin A in synaptic vesicle budding at the *Drosophila* neuromuscular junction. EMBO J. *21*, 1661–1672.
35. Jan, L.Y., and Jan, Y.N. (1976). Properties of the larval neuromuscular junction in *Drosophila melanogaster.* J. Physiol. *262*, 189–214.
36. Stewart, B.A., Atwood, H.L., Renger, J.J., Wang, J., and Wu, C.F. (1994). Improved stability of *Drosophila* larval neuromuscular preparations in haemolymph-like physiological solutions. J. Comp. Physiol. [A] *175*, 179–191.